

The Role of ^1H -MRS and ^{18}F FDG PET/CT in differentiating primary squamous cell carcinoma and metastatic Hodgkin's lymphoma in lung: An experimental pilot study

Marzieh Ebrahimi^{1,2}, Ahmad Bitarafan-Rajabi^{3,4}, Zeinab Paymani⁵, Armaghan Fard-Esfahani⁶, Siavash Kooranifar⁷, Arash Zare-Sadeghi^{1,2}, Samira Raminfard⁸, Mostafa Nazari⁵

¹Medical Physics Department, School of Medicine, Iran University of Medical Sciences, Tehran, Iran

²Fintech in Medicine Research Center, School of Medicine, Iran University of Medical Sciences, Tehran, Iran

³Echocardiography Research Center, Rajaie Cardiovascular Medical and Research Center, Iran University of Medical Sciences, Tehran, Iran

⁴Cardiovascular Interventional Research Center, Rajaie Cardiovascular Medical and Research Center, Iran University of Medical Sciences, Tehran, Iran

⁵Nuclear Medicine Department, Children Medical Center Hospital, Tehran University of Medical Sciences, Tehran, Iran

⁶Research Center for Nuclear Medicine, Tehran University of Medical Sciences, Tehran, Iran

⁷Hazrat-e Rasool Hospital, Iran University of Medical Sciences, Tehran, Iran

⁸Advanced Diagnostic and Interventional Radiology Research Center, Tehran University of Medical Sciences, Tehran, Iran

Corresponding author:

Dr. Ahmad Bitarafan-Rajabi

Department of Nuclear Medicine, Rajaie Cardiovascular Medical and Research Center, Iran University of Medical Sciences, Tehran, Iran

E-mail: bitarafan@hotmail.com

Running title: ^1H -MRS and ^{18}F FDG PET/CT in differentiating SCC and HL in lung cancer

Article History:

Received: 08 November 2023

Revised: 13 January 2024

Accepted: 14 January 2024

Published Online: 26 March 2024

ABSTRACT

Introduction: Distinguishing the cellular origin of lung cancer is essential for tailored patient care. This pioneering pilot study explores the synergy of ^1H -Magnetic Resonance Spectroscopy (^1H -MRS) and 2- ^{18}F fluoro-2-deoxy-D-glucose positron emission tomography/computed tomography (^{18}F FDG PET/CT) in the differentiation of primary squamous cell carcinoma (SCC) of the lung from Hodgkin's lymphoma (HL) metastases.

Methods: Ethically approved, the study enrolled 21 participants with confirmed lung lesions (10 SCC, 11 HL). ^{18}F FDG PET/CT and ^1H -MRS were conducted, and analyses were performed to assess diagnostic potential.

Results: Significant differences in [¹⁸F]FDG PET/CT parameters (SUV_{max} BSA, SUV_{max} LBM, and ID%) between SCC and HL were observed. Metabolite concentrations (Cho, Lac, Cr) from ¹H-MRS also exhibited distinctions. Correlations between PET values and metabolite concentrations hinted at links between glucose metabolism and molecular composition.

Conclusion: This study presents an innovative approach, integrating ¹H-MRS and [¹⁸F]FDG PET/CT to distinguish primary from metastatic lung lesions. The results hold promise for improving non-invasive diagnostic accuracy and guiding targeted therapies. Future research should validate these findings and explore the potential for clinical integration.

Keyword: Lung cancer differentiation; ¹H-MRS; [¹⁸F]FDG PET/CT; Squamous cell carcinoma; Hodgkin's lymphoma

INTRODUCTION

Lung tumors can be classified based on their origin. Tumors that originate within the lung tissue, such as squamous cell lung cancer (SCC), are referred to as primary, while those representing metastatic disease from other primary sites, such as Hodgkin's Lymphoma (HL) metastasis in the lung, are termed secondary. Lung metastases are observed in 35-55% of all cancer patients, exhibiting variability depending on the specific cancer type [1]. Particularly in the context of Hodgkin's Lymphoma (HL), lung involvement at the initial presentation is documented in 12% of patients [2]. Furthermore, the significance of secondary lung cancer development following Hodgkin's Lymphoma remains a noteworthy concern [3]. Lung tumors necessitate distinct management strategies and treatment approaches, ranging from surgical resection to systemic chemotherapy or targeted therapies, underscoring the importance of identifying the origin cell for effective treatment [4]. Accordingly, ensuring access to reliable diagnostic tools is crucial for devising effective treatment plans and conducting accurate prognostic evaluations. The conventional gold standard for determining the origin cells of lung lesion involves histopathological examination through biopsy. Nevertheless, given the invasive nature and associated risks of biopsies [5, 6], as well as the heterogeneity of tumoral masses, there is a growing interest in non-invasive imaging modalities to address these diagnostic challenges.

Currently, a reliable non-invasive method for determining the origin cells of lung cancer is unavailable. However, [¹⁸F]FDG PET/CT and CT have been used to evaluate pulmonary lesions, focusing on criteria such as size, shape, rate of growth, and nodule metabolism for diagnostic purposes; [¹⁸F]FDG PET/CT, predominantly assesses glucose uptake, while CT, mainly provides anatomical features [7-10]. ¹H-Magnetic Resonance Spectroscopy (¹H-MRS) also serves as an alternative non-invasive modality to clarify tumor histopathology [11]. ¹H-MRS is a specialized MRI technique with the potential to provide a more detailed insight into the metabolic characteristics of the lesions. It offers a noninvasive assessment of the general metabolic profile within malignant lesions, including concentrations of lactate (Lac), creatine (Cr), and choline (Cho), which play significant roles in cellular metabolism and oncogenesis [12-14]. These metabolites have been shown to play crucial roles in cellular metabolism and oncogenesis [15-18]. A multiparametric approach integrating ¹H-MRS with existing imaging modalities like [¹⁸F]FDG PET/CT may be particularly beneficial in cases where glucose uptake is not a reliable discriminator between different types of lesions to potentially enhance the diagnostic accuracy and/or facilitate possible targeted therapeutic interventions.

The objective of our study is to assess the individual and combined capabilities of ¹H-MRS and [¹⁸F]FDG PET/CT in differentiating between primary squamous cell lung cancer (SCC) and lung

metastases from Hodgkin's Lymphoma (HL). Our research aims to elucidate whether the metabolomic profile provided by ¹H-MRS and the glucose metabolism data offered by [¹⁸F]FDG PET/CT yield superior diagnostic accuracy in differentiating primary from secondary lung cancers, as a pilot study facilitating future non-invasive diagnostic approaches.

METHODS

Ethical considerations

This study was approved by the institutional Ethics Committee (IR.IUMS.FMD.REC.1399.546) and adhered to the 1964 Declaration of Helsinki and its later amendments. Informed written consent was obtained from all participants.

Study population

A cohort of 21 participants, comprised of 14 males (aged 16-81; mean: 48.00, SD: 21.77) and 7 females (aged 14-65; mean: 33.43, SD: ±18.00), were enrolled. Patients with pathology proven primary or secondary lung cancer were included. Participants exhibited biopsy-proven pulmonary malignant lesions including SCC (10 patients) and HL (11 patients), with no prior lung interventions such as surgery, radiotherapy, or chemotherapy.

[¹⁸F]FDG PET/CT imaging

Whole-body [¹⁸F]FDG PET-CT scans were acquired 60 minutes post intravenous administration of 5.5 MBq/Kg of [¹⁸F]FDG, utilizing a Siemens Biograph Horizon scanner. Low-dose CT scans were performed with CARE DOSE 4D algorithms for anatomical reference and attenuation correction. Scans had a spatial resolution of 1.2 mm, voltage range of 80-110 kVp, and current range of 50-80 mAs. PET images underwent time-of-flight (TOF) and point spread function (PSF) correction, reconstructed via OSEM algorithms (3 iterations, 10 subsets; matrix size 256x256), and smoothed with a Gaussian filter (FWHM 5 mm).

MRS acquisition

Single voxel spectroscopy (SVS) was conducted on a Siemens MAGNETOM AERA 1.5 Tesla scanner, employing an 8-channel phased array body coil and Syngo MR EII software. Respiratory trigger was used to counter thoracic motion. At first, a Turbo spin echo (TSE) sequence (repetition time (TR) = 502 mS, echo time (TE) = 58 mS, field of view (FOV) = 344x380, matrix = 320x224) generated T₁-weighted images. SVS was acquired via a Point Resolved Spectroscopy (PRESS) sequence (TR = 1200 mS, TE = 30 mS, voxel size ≥8 cm³, number of signal average (NSA) = 64). For outer volume suppression (OVS), six regional saturation bands were applied. B1 shim, transmitter, and water suppression were manually adjusted. Signals were acquired in raw data acquisition (RDA) format and processed with the Fast Fourier Transform (FFT) algorithm in TARQUIN (12) software.

Variables

Peak alignment was selected at chemical shifts of 1.33, 3, and 3.2 ppm for metabolites, specifically Lac, Cr, and Cho, respectively (Figure 1). The concentrations (molarity) of these metabolites were logarithmically scaled and reported in Table 1 to facilitate comparison across three distinct molar scales: >0.1 mM, 0.1 < mM <0.01, and <0.01 mM. The minimum detection threshold was determined below 0.001 mM and labeled as a negative peak.

In the case of [¹⁸F]FDG PET/CT, three different maximum standardized uptake value (SUV_{max}) metrics were evaluated for each lesion: SUV_{BW} based on body weight, SUV_{BSA} based on body surface area, SUV_{LBM} based on lean body mass, and injected dose percentage (ID%).

Statistical analysis

Descriptive analyses including mean and standard deviation (SD) of variables, as well as combined analysis incorporating both PET and MRS data was conducted to explore whether the integration of metabolic and functional data could enhance the differentiation between primary (SCC) and metastatic lung (HL) lesions. For statistical comparisons, the Mann-Whitney U test was utilized to evaluate the mean differences in the aforementioned parameters between primary and metastatic lesions. Additionally, correlation between variables was determined using Spearman's correlation coefficient (r). The statistical software SPSS v.22 was utilized for these analyses. A significance level of $p < 0.05$ was considered statistically significant.

RESULTS

The first cohort group included 10 patients with histologically confirmed lung SCC (10 males, 4 females, mean age 64.78 ± 9.42 years), comprising a total of 14 primary malignant lesions. Second group included 11 patients (7 males, 8 females, mean age 22.46 ± 7.48 years) with a total of 15 metastatic pulmonary lesions. Table 1 presents the collected data, which includes histopathologic assessments, semi-quantitative measurements from [¹⁸F]FDG PET/CT scans (Figure 2), anatomical lesion locations, as well as maximum and minimum lesion diameters and Cho, Lac and Cr concentration.

The mean and SD of the $SUV_{max BW}$, $SUV_{max BSA}$, $SUV_{max LBM}$, and ID% for HL patients were as follows: (6.97 ± 2.59), (1.79 ± 0.74), (4.14 ± 1.99), and (6.70 ± 2.20), respectively. In contrast, the corresponding values for SCC patients were higher: $SUV_{max BW}$ (10.23 ± 4.84), $SUV_{max BSA}$ (2.99 ± 1.47), $SUV_{max LBM}$ (8.49 ± 4.26), and ID% (45.83 ± 27.30).

The Mann-Whitney U test revealed significant differences in $SUV_{max BSA}$, $SUV_{max LBM}$, and ID% values between the SCC and HL groups ($SUV_{max BSA}$: $U = 47.00$, $p = 0.012$; $SUV_{max LBM}$: $U = 56.00$, $p = 0.032$; ID%: $U = 0.00$, $p = 0.001$). However, there was no statistically significant difference observed in $SUV_{max BW}$ values between the two groups ($p = 0.67$).

This study revealed that the maximum concentration of Cho, Lac, and Cr in HL patients ranged from 0.01 to 0.1 mM, with the following frequencies: Cho = Lac (53.3%) and Cr occurred at a rate of 13.3%. In contrast, SCC patients exhibited a higher occurrence of Cho, Lac, and Cr peaks exceeding 0.1 mM, with frequencies of 71.4%, 28.6%, and 42.9%, respectively.

Notably, Cho and Lac peaks were absent in 13.3% of HL patients, and 40% of HL patients lacked a Cr peak. In contrast, these peak absences were not observed in SCC patients.

It is considerable that the Mann-Whitney U test revealed significant differences in lactate, choline, and creatine values between the SCC and HL groups (lactate: $U = 53.00$, $p = 0.036$; choline: $U = 35.00$, $p = 0.04$; creatine: $U = 8.00$, $p = 0.001$).

A Spearman correlation analysis was conducted to examine the association between PET semi-quantification values and the concentrations of Cho, Lac, and Cr. The results demonstrated a statistically significant positive correlation between PET semi-quantification values and the concentrations of Cho ($\rho = 0.73$, $p < 0.004$) and Cr ($\rho = 0.72$, $p < 0.027$) in the HL group. No correlation was observed for Lac levels. Furthermore, in the SCC group, there was a statistically significant positive correlation between the semi-quantification values and the concentrations of

Cho ($\rho = 0.63$, $p < 0.017$), Lac ($\rho = 0.57$, $p < 0.032$), and Cr ($\rho = 0.609$, $p < 0.021$). These findings suggest a potential link between the glucose metabolism activity captured by PET imaging and the levels of Cho, Lac, and Cr in the pulmonary lesions.

DISCUSSION

In this study we assessed the diagnostic utility of $^1\text{H-MRS}$ and $^{18}\text{F}]\text{FDG PET/CT}$ in differentiating pulmonary malignant lesions showing different metabolic profiles in SCC versus HL, such as increased lactate levels and heightened glycolytic activity, being compatible with more aggressive malignant nature of SCC. The results support the hypothesis that these imaging techniques, individually and in combination, can provide valuable insights for diagnosis and treatment planning.

The Mann-Whitney U test results demonstrated significant differences in both SUV measurements and metabolite concentrations between SCC and HL groups ($p < 0.05$). The SCC lesion showed higher SUV values and Lac, Cho, and Cr concentrations compared to HL. Additionally, the Spearman correlation analysis revealed positive correlations ($r > 0.57$) between PET measurements and Cho, Cr, and Lac concentrations in both types of malignancy. This suggests that integrating metabolic data from $^1\text{H-MRS}$ with functional data from $^{18}\text{F}]\text{FDG PET/CT}$ could yield a more accurate diagnosis.

Incorporating data from our study, the observed SUV measurements of 6.9 for Hodgkin's lymphoma are aligned with findings from other studies. For instance, Nagaraj Holalkere's research [19] reported a mean SUV_{max} of 6.1 for classical and 10.1 for non-classical Hodgkin lymphoma, emphasizing the distinctions in $^{18}\text{F}]\text{FDG}$ avidity among these subtypes. Furthermore, Li Hongling's investigation [20] contributed valuable insights by encompassing 103 patients revealing significant differences in SUV_{max} mean \pm SD. Their study demonstrated that non-Hodgkin lymphoma exhibited a higher SUV_{max} (9.8 ± 6.0) compared to Hodgkin lymphoma (7.5 ± 2.8).

Dijkman et al. reported SUVs from $^{18}\text{F}]\text{FDG PET/CT}$ images can be helpful in differentiating metastatic disease from primary tumors with AUC of 0.81% in patients with pulmonary lesions [21]. Ghossein and colleagues investigated the utility of $^{18}\text{F}]\text{FDG}$ uptake intensity in distinguishing primary lung cancers from secondary lung lesions in patients with a solitary malignant pulmonary lesion (SMPL) and a previously removed extrapulmonary tumor. They utilized $\text{SUV}_{\text{max}} \text{ SMPL} / \text{SUV}_{\text{max}} \text{ Liver}$ ratios and correlated them with extrapulmonary tumor grades. Their study found that 60% of cases exhibited discordant results between $^{18}\text{F}]\text{FDG}$ uptake and extrapulmonary tumor grade, with 81% of these cases correctly identified as primary lung cancers. These initial results suggest that a mismatch between SMPL/Liver SUV_{max} and extrapulmonary tumor grade could effectively differentiate primary lung cancer from metastases [10].

$^1\text{H-MRS}$ in lung cancer diagnostics remains largely unexplored due to inherent challenges specific to lung tissue analysis. The unique characteristics of the lung, including air-filled spaces, respiratory motion, and low tissue density, pose substantial technical hurdles for acquiring precise metabolic information through MRS. These complexities significantly affect signal intensity, potentially leading to artifacts and hindering the accurate interpretation of metabolic profiles. However, results of $^1\text{H-MRS}$ have demonstrated that lung cancer mass has higher Lac and Cho signals than those of normal tissues [22]. As well, Cho levels were significantly higher in malignant lesions compared with benign lesions. However, according to our knowledge, there is no study clarifying the $^1\text{H-MRS}$ role in differentiating the cellular origin of the lung tumors. $^1\text{H-}$

MRS utility has been well-documented in neuro-oncology; several studies have effectively employed ¹H-MRS to differentiate between high-grade gliomas and metastatic brain tumors, focusing particularly on intertumoral Cr levels as a distinguishing biomarker [23, 24]. In primary brain tumors like gliomas, Cr is typically present; conversely, absent Cr peak can indicate cerebral metastasis. This dichotomy in Cr levels is thought to stem from the differential metabolic pathways active in primary versus secondary brain tumors [25].

There are some limitations to consider. Mainly, this was a pilot experiment with relatively small sample size, which could affect the generalizability of the findings. Further research is needed to validate the diagnostic criteria derived from this study across larger, diverse patient populations and different imaging platforms.

CONCLUSION

In conclusion, our pilot study provides compelling evidence for the combined application of ¹H-MRS and [¹⁸F]FDG PET/CT in differentiating between primary SCC and metastatic HL pulmonary lesions. The analysis of molecular composition levels and metabolic activity patterns holds promise for effectively discriminating between primary lung SCC and metastatic HL. Future research should focus on the prospective validation of these findings and explore the potential of integrating these imaging modalities into routine clinical practice for more targeted therapeutic interventions.

Acknowledgement

The authors would like to express their gratitude to all those who helped throughout the study. It is important to note that no specific organization provided any funding for this research.

REFERENCES

1. Crow J, Slavin G, Kreel L. Pulmonary metastasis: a pathologic and radiologic study. *Cancer*. 1981;47(11):2595-602.
2. Lee KS, Kim Y, Primack SL. Imaging of pulmonary lymphomas. *AJR Am J Roentgenol*. 1997 Feb;168(2):339-45.
3. Lorigan P, Radford J, Howell A, Thatcher N. Lung cancer after treatment for Hodgkin's lymphoma: a systematic review. *Lancet Oncol*. 2005 Oct;6(10):773-9.
4. Fisseler-Eckhoff A, Müller KM. Differentialdiagnose primärer Lungentumoren und pulmonaler Metastasen [Differential diagnosis of primary lung tumors and pulmonary metastases]. *Verh Dtsch Ges Pathol*. 2000;84:106-17.
5. Zhang Y, Shi L, Simoff MJ, J Wagner O, Lavin J. Biopsy frequency and complications among lung cancer patients in the United States. *Lung Cancer Manag*. 2020 Aug 17;9(4):LMT40.
6. Vachani A, Zhou M, Ghosh S, Zhang S, Szapary P, Gaurav D, Kalsekar I. Complications after transthoracic needle biopsy of pulmonary nodules: a population-level retrospective cohort analysis. *J Am Coll Radiol*. 2022 Oct;19(10):1121-9.
7. Snoeckx A, Reyntiens P, Desbuquoit D, Spinhoven MJ, Van Schil PE, van Meerbeeck JP, Parizel PM. Evaluation of the solitary pulmonary nodule: size matters, but do not ignore the power of morphology. *Insights Imaging*. 2018 Feb;9(1):73-86.

8. Christensen JA, Nathan MA, Mullan BP, Hartman TE, Swensen SJ, Lowe VJ. Characterization of the solitary pulmonary nodule: 18F-FDG PET versus nodule-enhancement CT. *AJR Am J Roentgenol*. 2006 Nov;187(5):1361-7.
9. Groheux D, Quere G, Blanc E, Lemarignier C, Vercellino L, de Margerie-Mellon C, Merlet P, Querellou S. FDG PET-CT for solitary pulmonary nodule and lung cancer: Literature review. *Diagn Interv Imaging*. 2016 Oct;97(10):1003-1017.
10. Ghossein J, Gingras S, Zeng W. Differentiating primary from secondary lung cancer with FDG PET/CT and extra-pulmonary tumor grade. *J Med Imaging Radiat Sci*. 2023 Sep;54(3):451-456.
11. Kugel H, Heindel W, Ernestus RI, Bunke J, du Mesnil R, Friedmann G. Human brain tumors: spectral patterns detected with localized H-1 MR spectroscopy. *Radiology*. 1992 Jun;183(3):701-9.
12. Kannampuzha S, Mukherjee AG, Wanjari UR, Gopalakrishnan AV, Murali R, Namachivayam A, Renu K, Dey A, Vellingiri B, Madhyastha H, Ganesan R. A Systematic role of metabolomics, metabolic pathways, and chemical metabolism in lung cancer. *Vaccines (Basel)*. 2023 Feb 7;11(2):381.
13. Madama D, Martins R, Pires AS, Botelho MF, Alves MG, Abrantes AM, Cordeiro CR. Metabolomic profiling in lung cancer: a systematic review. *Metabolites*. 2021 Sep 17;11(9):630.
14. Liang S, Cao X, Wang Y, Leng P, Wen X, Xie G, Luo H, Yu R. Metabolomics analysis and diagnosis of lung cancer: insights from diverse sample types. *Int J Med Sci*. 2024 Jan 1;21(2):234-52.
15. Mountford CE, Doran S, Lean CL, Russell P. Proton MRS can determine the pathology of human cancers with a high level of accuracy. *Chem Rev*. 2004 Aug;104(8):3677-704.
16. Panebianco V, Giove F, Barchetti F, Podo F, Passariello R. High-field PET/MRI and MRS: potential clinical and research applications. *Clin Transl Imaging*. 2013;1(1):17-29.
17. Panigrahy A, Nelson MD Jr, Blüml S. Magnetic resonance spectroscopy in pediatric neuroradiology: clinical and research applications. *Pediatr Radiol*. 2010 Jan;40(1):3-30.
18. Hollingworth W, Medina LS, Lenkinski RE, Shibata DK, Bernal B, Zurakowski D, Comstock B, Jarvik JG. A systematic literature review of magnetic resonance spectroscopy for the characterization of brain tumors. *AJNR Am J Neuroradiol*. 2006 Aug;27(7):1404-11.
19. Holalkere N, Hochberg EP, Takvorian R, Blake M, Toomey C, Michaelson J, Rahemtullah A, Abramson JS. Intensity of FDG uptake on PET scan varies by histologic subtype of hodgkin lymphoma. *Blood*. 2007;110(11):4393.
20. Li H, Wang X, Zhang L, Yi X, Qiao Y, Jin Q. Correlations between maximum standardized uptake value measured via ¹⁸F-fluorodeoxyglucose positron emission tomography/computed tomography and clinical variables and biochemical indicators in adult lymphoma. *J Cancer Res Ther*. 2019;15(7):1581-8.
21. Dijkman BG, Schuurbiens OC, Vriens D, Looijen-Salamon M, Bussink J, Timmer-Bonte JN, Snoeren MM, Oyen WJ, van der Heijden HF, de Geus-Oei LF. The role of (18)F-FDG PET in the differentiation between lung metastases and synchronous second primary lung tumours. *Eur J Nucl Med Mol Imaging*. 2010 Nov;37(11):2037-47.

22. Fujimoto S, Minato K, Horikoshi H, Suga S, Sato M, Mashimo K, Onozato R, Fujita A. Proton magnetic resonance spectroscopy of lung cancer in vivo. *Radiol Case Rep.* 2020 May 22;15(7):1099-102.
23. Csutak C, Ștefan PA, Lenghel LM, Moroșanu CO, Lupean RA, Șimonca L, Mișu CM, Lebovici A. Differentiating high-grade gliomas from brain metastases at magnetic resonance: the role of texture analysis of the peritumoral zone. *Brain Sci.* 2020 Sep 16;10(9):638.
24. Law M, Cha S, Knopp EA, Johnson G, Arnett J, Litt AW. High-grade gliomas and solitary metastases: differentiation by using perfusion and proton spectroscopic MR imaging. *Radiology.* 2002 Mar;222(3):715-21.
25. Ishimaru H, Morikawa M, Iwanaga S, Kaminogo M, Ochi M, Hayashi K. Differentiation between high-grade glioma and metastatic brain tumor using single-voxel proton MR spectroscopy. *Eur Radiol.* 2001;11(9):1784-91.

Table 1. Summary of clinical and metabolic parameters in lung lesions

Lesion Code	Age (year)	Gender	Lung Pathology	Localization & Lesion Size (mm) (Maximum*Minimum)	PET Quantification Values				Peak Presence and Concentration (mM)		
					SUV _{max} BW	SUV _{max} BSA	SUV _{max} LBM	ID%	Choline	Lactate	Creatine
1	27	F	HL	Right middle lobe (lateral segment & 70*42)	8.35	2.04	6.45	9.13	0.01 <> 0.1	0.01 <> 0.1	< 0.01
2	36	F	HL	Right upper lobe (posterior segment & 56*49)	5.21	1.28	4.02	5.7	< 0.01	< 0.01	-
3	21	F	HL	Right lower lobe (superior segment & 68*51)	6.44	1.58	4.97	7.05	0.01 <> 0.1	0.01 <> 0.1	-
4	21	F	HL	Right lower lobe (anterior segment & 93*45)	6.36	1.56	4.91	6.96	0.01 <> 0.1	0.01 <> 0.1	-
5	23	M	HL	Left upper lobe (superior-ligular segment & 83*67)	8.28	2.03	6.39	9.06	0.01 <> 0.1	0.01 <> 0.1	< 0.01
6	19	M	HL	Left upper lobe (apico-posterior segment & 94*73)	6.68	1.64	5.16	7.31	0.01 <> 0.1	0.01 <> 0.1	< 0.01
7	33	M	HL	Left upper lobe (anterior segment & 77*59)	4.71	1.15	3.63	5.15	< 0.01	< 0.01	-
8	20	M	HL	Left lower lobe (posterior segment & 120*85)	7.05	1.73	5.44	7.71	0.01 <> 0.1	0.01 <> 0.1	< 0.01
9	20	M	HL	Left lower lobe (apico-lateral segment & 170*31)	7.99	1.96	6.17	8.74	0.01 <> 0.1	0.01 <> 0.1	< 0.01
10	39	M	HL	Left upper lobe (anterior segment & 55*63)	8.23	2.02	3.36	9	0.01 <> 0.1	0.01 <> 0.1	-
11	16	M	HL	Right upper lobe (anterior segment & 42*41)	3.88	0.95	2.99	4.24	< 0.01	< 0.01	-
12	17	F	HL	Right upper lobe (apical segment & 25*14)	3.35	0.95	2.51	2.16	-	-	< 0.01
13	17	F	HL	Right middle lobe (lateral segment & 37*28)	3.84	1.09	2.9	2.51	-	-	< 0.01
14	14	F	HL	Right upper lobe (superior segment & 46*32)	12.35	3.5	9.31	8.06	0.01 <> 0.1	< 0.01	0.01 <> 0.1
15	14	F	HL	Right upper lobe (lateral segment & 66*64)	11.89	3.38	8.98	7.76	0.01 <> 0.1	< 0.01	0.01 <> 0.1
16	51	M	SCC	Right upper lobe (apical segment & 51*49)	3.8	1.15	3.28	19.33	0.01 <> 0.1	0.01 <> 0.1	0.01 <> 0.1
17	63	M	SCC	Right lower lobe (posterior segment & 84*52)	3.38	1.02	2.92	17.2	0.01 <> 0.1	0.01 <> 0.1	0.01 <> 0.1
18	74	M	SCC	Right lower lobe (anterior segment & 99*64)	4.03	1.21	3.48	20.48	> 0.1	> 0.1	0.01 <> 0.1
19	68	M	SCC	Left upper lobe (anterior segment & 45*31)	12.24	3.69	10.57	62.26	> 0.1	> 0.1	> 0.1
20	55	M	SCC	Right middle lobe (lateral segment & 83*51)	13.56	4.09	11.71	68.99	> 0.1	> 0.1	> 0.1

21	55	M	SCC	Right lower lobe (lateral segment & 72*47)	13.55	4.09	11.71	68.93	> 0.1	> 0.1	0.01 <> 0.1
22	61	M	SCC	Right middle lobe (lateral segment & 104*61)	7.92	2.39	6.84	33.18	0.01 <> 0.1	> 0.1	> 0.1
23	81	M	SCC	left upper lobe (anterior segment & 193*124)	18.22	5.49	15.73	92.65	> 0.1	> 0.1	> 0.1
24	81	M	SCC	Right lower lobe (superior segment & 231*89)	19.66	5.93	16.98	100	> 0.1	> 0.1	> 0.1
25	69	M	SCC	left upper lobe (apico-posterior segment & 135*44)	10.39	3.13	8.97	52.83	> 0.1	> 0.1	> 0.1
26	54	F	SCC	Right lower lobe (posterior segment & 74*68)	12.19	3.22	8.77	34.79	> 0.1	0.01 <> 0.1	0.01 <> 0.1
27	65	F	SCC	Right middle lobe (lateral segment & 92*77)	8.45	2.23	6.08	24.13	> 0.1	0.01 <> 0.1	0.01 <> 0.1
28	65	F	SCC	Right lower lobe (posterior segment & 49*23)	8.06	2.27	6.19	24.56	> 0.1	0.01 <> 0.1	0.01 <> 0.1
29	65	F	SCC	Right lower lobe (lateral segment & 27*26)	7.84	2.07	5.64	22.37	> 0.1	0.01 <> 0.1	0.01 <> 0.1

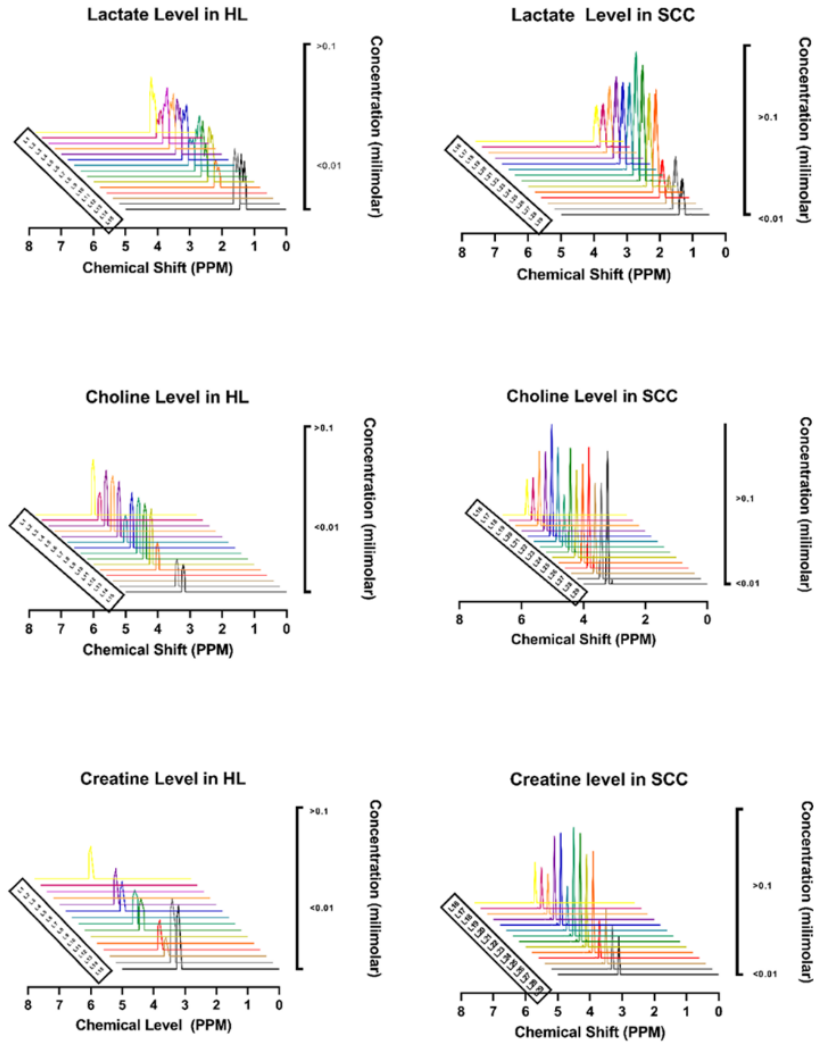


Fig 1. Metabolic profiles of choline, lactate, and creatine in squamous cell carcinoma (SCC) and Hodgkin lymphoma (HL) Lesions. This figure illustrates variations in metabolite concentrations and their absences in HL compared to SCC, providing valuable insights into the distinctive metabolic profiles of SCC and HL

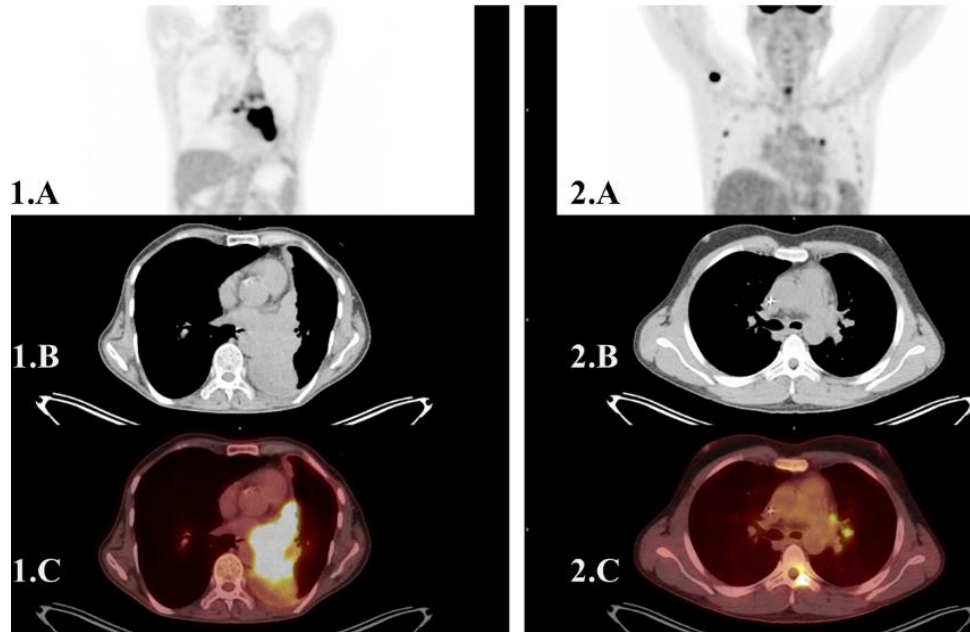


Fig 2. PET/CT images of two patients. 1.A. MIP image of [^{18}F]FDG PET scans of a patient with histopathological proved SCC mass in lung. 1.B. Axial CT slice of the chest show a mass in the medial aspect of left pulmonary lower lobe. 1.C. Co-Reregistered axial [^{18}F]FDG PET/CT Slice shows heterogenous increased uptake in mass; 2.A. MIP image of [^{18}F]FDG PET scans of a patient with histopathological proved Hodgkin's lymphoma lesion in the hilum of the left lung. 2.B. Axial CT slice of the chest shows lesions in the left pulmonary region. 2.C. Axial [^{18}F]FDG PET/CT with increased uptake in lesions